Temperature-dependent nucleation and capture-zone scaling of C_{60} on silicon oxide

M.A. Groce, B.R. Conrad [1], W.G. Cullen, A. Pimpinelli [2], E.D. Williams [3], T.L. Einstein *

Department of Physics & MRSEC, University of Maryland, College Park, MD 20742-4111, USA

ARTICLE INFO

ABSTRACT

Submonolayer films of C_{60} have been deposited on ultrathin SiO_2 films for the purpose of characterizing the initial stages of nucleation and growth as a function of temperature. Capture zones extracted from the initial film morphology were analyzed using both the gamma and generalized Wigner distributions. The calculated critical nucleus size i of the C_{60} islands was observed to change over the temperature range 298 K to 483 K. All fitted values of i were found to be between 0 and 1, representing stable monomers and stable dimers, respectively. With increasing temperature of film preparation, we observed i first increasing through this range and then decreasing. We discuss possible explanations of this reentrant-like behavior.

© 2011 Elsevier B.V. All rights reserved.

1. Introduction

The C_{60} molecule is interesting in part because of its elegant structure. Consisting of 60 carbon atoms arranged in a truncated icosahedron, approximating a hollow sphere, its symmetry and uniform composition provide a model system for studying the basic mechanisms underlying the diffusion and nucleation of particles on a surface. Practically, C_{60} and its derivatives display modest charge carrier mobilities in neat (pure, single-component) organic transistors [1] and are used in the standard organic photovoltaic heterostructure, P3HT/PCBM [2]. Fundamental studies of these devices can be complicated by unknown or complex film morphology since the detailed molecular order significantly impacts device characteristics [2–4]. Exploring the initial nucleation mechanisms that influence film growth, and which ultimately determine device performance, is necessary to further our ability to model such systems and control device optimization.

The structural and electronic properties of C_{60} films have been studied in the context of single crystals [5,6], bilayer structures [7,8], and neat devices [9,10] typically hundreds of nanometers thick. However, to the best of our knowledge the subtleties of the early nucleation stage have not been examined. Specifically, high-resolution imaging of C_{60} films on insulating oxide surfaces, required to model the growth kinetics of device-relevant films, have not previously been achieved. Oxide thickness – typically several hundred nanometers in devices – precludes the use of scanning tunneling microscopy (STM) since the tunneling current would be too low to measure. By employing an ultra-thin oxide (UTO) ~1 nm thick, we can retain the ability to image individual molecules on a surface with chemical properties similar to those of the thicker oxides.

In this paper, we present the results of growing C_{60} films while holding the substrates at temperatures ranging from room temperature (298 K) to 483 K. We apply capture-zone scaling to STM topography data and observe that the extracted critical nucleus size behaves parabolically, first increasing, then decreasing. We argue that the most likely explanation of this unorthodox behavior is surface defects.

2. Materials and methods

The experiments were performed in an ultrahigh vacuum (UHV) chamber with base pressure ~4×10^{-11} Torr and equipped with a variable temperature scanning tunneling microscope (Omicron VT-STM). The substrates were prepared from n-doped Si(111) wafers with resistivity between 0.01–0.04 $\Omega \cdot cm$, misoriented 0.1° toward the [211] direction. The silicon was cleaned according to established recipes with repeated flashing at 1523 K, followed by slow cooling through the (1×1) to (7×7) phase transition [11]. The presence of the (7×7) reconstruction was confirmed using STM. An ultra-thin oxide layer was then grown by exposing the room temperature Si substrate to 2.5×10^6 L of O_2 in an attached chamber with a base

---

* Corresponding author. Tel.: +1 301 405 6147; fax: +1 301 314 9465.
E-mail addresses: mzimm@umd.edu (M.A. Groce), conradbr@appstate.edu (B.R. Conrad), wcullen@umd.edu (W.G. Cullen), apimpin1@umd.edu (A. Pimpinelli), edw@umd.edu (E.D. Williams), einstein@umd.edu (T.L. Einstein).
[1] Present and permanent address: Dept. of Physics and Astronomy, Appalachian State University, 525 Rivers Street, Boone, NC 28608, USA.
[2] Also: Scientific Attaché, French Embassy in the US, Consulate General of France, Houston, Texas 77056. On leave from: LASMEA, UMR 6602 CNRS/Université Blaise Pascal, Clermont 2, F-63177 Aubière cedex, France.
[3] Present address: Chief Scientist, BP p.l.c., 1 St. James Square, London SW1Y 4PD, UK.
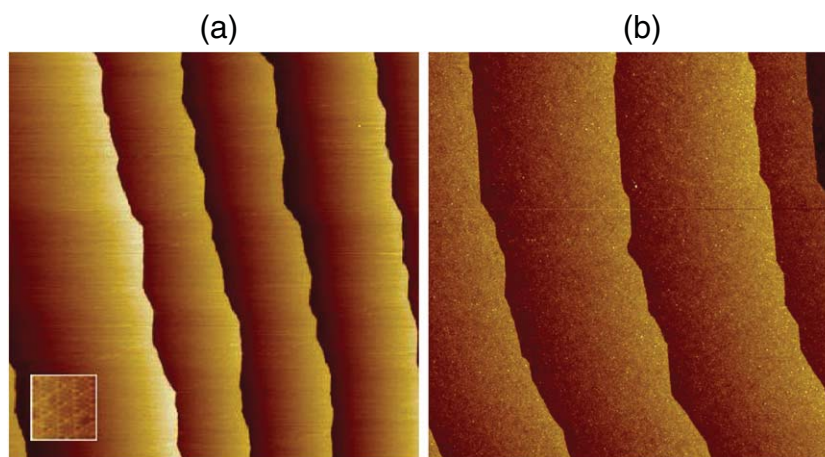
(a)   (b)

Fig. 1. $(1~\mu m)^2$ STM topography image (I = 100 pA, V = +2.5 V, 1.95 nm/pixel) of: (a) pristine Si(111)-(7×7) surface. The lines propagating vertically through the image are single atomic Si steps 0.32 nm in height. The (7×7) pattern is not resolvable at this magnification, but is evident in the enlargement of a 7 nm×7 nm region shown in the small inset. (b) Si substrate with ultra-thin oxide layer. Vertical Si steps are still visible, but the (7×7) reconstruction is no longer observed.

pressure < 10^{-9} Torr at room temperature. The sample was outgassed at 573 K in UHV to remove excess surface species.

Fig. 1 compares the clean silicon surface to the surface of the ultra-thin silicon oxide. The oxide has a rougher appearance, with the brightest features appearing to be ~0.1 nm tall. However, because STM measures height by measuring tunneling current, regions with higher conductivity will have greater apparent heights. Bright features on the oxide surface actually correspond to thinner regions of the oxide film, while darker spots correspond to thicker oxide [12,13].

C_{60} films were immediately grown via physical vapor deposition from an effusion cell attached to the main UHV chamber. The effusion cell was operated at a flux rate of 0.3 monolayers (ML)/min as calibrated for a close-packed film of C_{60} on Ag(111). Each film was prepared with 0.1 ML of C_{60} via timed exposure to the effusion cell. Substrates were held at temperatures ranging from room temperature (298 K) to 483 K during the entire deposition. Unit sticking coefficient was assumed. Fractional coverages were corroborated by doing grain analysis using Scanning Probe Image Processor (SPIP™) software. Higher temperatures were not explored in this experiment in order to avoid chemical reactions involving C_{60}. The films were allowed to return to room temperature before measurement by STM with chemically etched tungsten tips. All images were taken in constant-current mode with a current setpoint of 70–100 pA and a sample bias of +2.5 V.
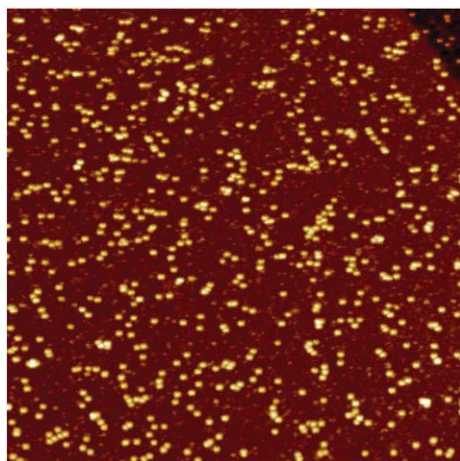

Fig. 2. A typical $(100~nm)^2$ STM topography image showing C_{60} molecules on ultra-thin SiO_2 (I = 100 pA, V = +2.5 V, 0.20 nm/pixel). The film was prepared at 333 K. A single silicon step edge is visible in the upper right corner.

A characteristic image of a 0.1 ML C_{60} deposition on the UTO substrate is shown in Fig. 2. The apparent molecule diameter, obtained by measuring the full width at half maximum of a topography peak, is ~1.3 nm. This is modestly larger than the established diameter of 1 nm [14], due to the finite size of the STM tip [15]. C_{60} islands were measured by applying a height threshold to the images, along with a minimum island area to eliminate false positives resulting from image noise. While many of the molecules are isolated, there is a distribution of clusters ranging from 2 to at least 15 molecules. The observed islands are all two-dimensional, though they are not compact, show no internal order, and should not be considered crystalline. The typical distance between the centers of C_{60} molecules in an island is ~1.5 nm.

3. Calculation

A common model to characterize the initial nucleation and growth of deposited films is via the critical nucleus size i. The value of i reflects the number of particles in the largest unstable island. Thus, $i = 0$ corresponds to the case of stable monomers, $i = 1$ describes stable dimer formation, and so on. There exists a unique relationship between i and the island size distribution (ISD) [16], though the precise nature of that relationship is still under study [17]. The critical nucleus size has been investigated in the context of kinetic Monte Carlo (KMC) simulations, examining how varying functions of i fit the simulated ISD [18]. More recently, the capture zone distribution (CZD) has been used in place of the ISD [19]. A capture zone is a Voronoi polygon drawn around the center of mass of an island, and represents the set of points closer to that island than to any other (i.e., a proximity or generalized Wigner–Seitz cell).[4]

A distribution commonly used to describe CZDs is the single-parameter gamma distribution (ΓD), which reflects the area distribution of Voronoi cells constructed from points randomly placed in a plane [19,20]:

$$G_\alpha(s) = \frac{(\alpha)^\alpha}{\Gamma(\alpha)} s^{\alpha-1} e^{-\alpha s} \qquad (1)$$

where s is the capture zone area divided by its mean and α is the "shape parameter" [21] (to which the "inverse rate parameter" in the exponent is equal for unit mean, yielding this single-parameter expression). This

---

[4] While the ISD and CZD use different physical measures to describe island growth, they generally give qualitatively similar single-peak distributions; however, the CZD always vanishes as the capture zone size goes to zero, while there may be a large numbers of small islands,
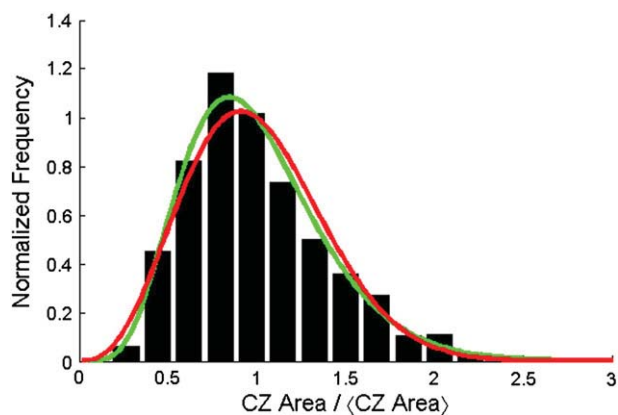
Fig. 3. An example capture zone distribution (CZD) histogram corresponding to islands grown at 328 K. The red/black curve shows the GWD fit ($i = 0.6 \pm 0.2$) and the green/gray curve shows the gamma distribution fit ($i = 0.7 \pm 0.2$). (For interpretation of the references to color in this figure legend, the reader is referred to the web version of this article.)

Table 1
Capture zone distribution fitting parameters α from Eq. (1) and β from Eq. (2) at each deposition temperature. For GWD the critical nucleus size i is obtained from $i = \beta - 2$; for the ΓD it is based on the similarity between $G_{2\beta+1}$ and $P_\beta(s)$ in the central region of the distribution, whence $i = (\alpha - 5)/2$. N_{isl} is the island density in units of # islands/nm².

Temperature (K)	ΓD α	ΓD i	GWD β	GWD i	N_{isl}
298	5.7 ± 0.4	0.4 ± 0.2	2.2 ± 0.2	0.2 ± 0.2	0.039
328	6.4 ± 0.3	0.7 ± 0.2	2.6 ± 0.2	0.6 ± 0.2	0.040
373	6.8 ± 0.4	0.9 ± 0.2	2.9 ± 0.2	0.9 ± 0.2	0.050
423	6.8 ± 0.3	0.9 ± 0.2	2.8 ± 0.2	0.8 ± 0.2	0.043
483	5.3 ± 0.3	0.2 ± 0.2	2.1 ± 0.2	0.1 ± 0.2	0.048

distribution was invoked long ago to characterize interstellar dust [22] and was adopted in some extensive work on foams and froths [20]. In 2007 the generalized Wigner distribution was introduced as an alternative way to model the CZD, since it was shown to account for CZDs from simulated and experimental data at least as well as the gamma distribution [23]. The GWD has been successfully used to describe other spacing fluctuation phenomena in cases where there is a slight correlation between nucleation centers [24]; this is an advantage over the ΓD approach since island nucleation is not a completely random process. This single-parameter distribution takes the form

$$P_\beta(s) = a_\beta s^\beta \exp\left(-b_\beta s^2\right), \tag{2}$$

where s is again the CZ area divided by the mean CZ area and β is the characteristic exponent. The terms a_β and b_β are β-dependent constants[5] that enforce that $P_\beta(s)$ is normalized and has unit mean. Through a mean field argument, Ref. [23] proposed that s could be directly related to i; specifically it was argued that $\beta = i + 1$ [23]. Recent work indicates that one must go beyond mean field, which leads to the modification $\beta \approx i + 2$ [25–28].

By virtue of the similarity of $P_{i+2}(s)$ and $G_{2i+5}(s)$ over the region near $\frac{1}{2} < s < 2$, where the statistics are best, the exponent α can likewise be taken as a function of the critical nucleus size i, even though there is no physical argument for this association. Recent studies of CZDs based on compilations of KMC results make use of the idea that the dimensionless parameter $\alpha \approx 2i + 5$ [26,29]. Note that the initial power-law dependence is different, with $P_\beta(s) \propto s^{i+2}$ while $G_\alpha(s) \propto s^{2i+4}$ with an exponent twice as large; correspondingly, for large capture zone area s the former decays as a Gaussian while the latter decays exponentially.

4. Results and discussion

Through least-squares fits applying each functional form to our measurements of capture zones at various growth temperatures, we extract values of parameters α and β, from which we determine i. Fig. 3 shows an example histogram of the measured CZD from the film grown at 423 K, along with the ΓD and GWD fits. The histograms are based on ~1000 individual islands measured at each temperature. The curves generated by fitting each model to the histograms are very similar, as are the resulting error bars on the parameters; quantitative

statistical tests of fit are essentially the same. (The gamma distribution does tend to have a higher peak than the generalized Wigner form which may be visually appealing.) Our sample sizes are not large enough to rule out either model. Another experiment has also found either fitting function adequate[6] [30]. All values of fitting parameters β and α, along with their standard errors, and the resulting calculated values for critical nucleus size i are shown in Table 1. On the scale of the error bars, these results are insensitive to variations in bin size.

The plot of critical nucleus size i versus temperature in Fig. 4 includes the values from both models applied to each of the histograms. Error bars illustrate that the ΓD and GWD produced i values within one standard deviation of each other. Noninteger values for i reveal the heuristic nature of the critical nucleus size, but may be understood as a reflection of the detachment probability for a quasi-stable island of the next larger integer number of molecules [31]. Rather than a monotonic dependence of i on temperature, the trend seen in Fig. 4 shows a parabolic-shaped increase followed by a decrease. The peak of a least-squares-fitted parabola lies between 383–389 K with 95% confidence.

To gain some understanding of this curious behavior, we tabulated the island densities N_{isl} at the five temperatures at which we fit distributions, listed in the rightmost column of Table 1. For nucleated growth in pure systems, N_{isl} is expected to decrease rapidly as temperature rises, as in Fig. 4b of Ref. [32]. Instead, we find little systematic variation with increasing temperature (if anything, a slight increase). Such behavior could arise when defects or impurities play a significant role. In this regard, our substrate, as noted in Section 2, is not a flat facet but instead is rather irregular, so there is intrinsically a variation of binding sites such as might be produced by defects. Note that this complication did not hinder extraction of meaningful exponents from analysis of the CZD for pentacene on the same substrate with various dilute concentrations of pentacenequinone impurities [33].

Further evidence in support of this picture comes from the observation that the preponderance of islands, at some temperatures up to ¾, are monomers. In many analyses, monomers are excluded from the calculation of capture zones since the monomers are viewed as the fundamental mobile species. If we do this, the statistics are severely degraded, so that many of the results become unreliable, but invariably the deduced value of β decreases by about 0.4, and the value of i is roughly zero. It is hard to rationalize this behavior in terms of a homogeneous nucleation picture, but it is consistent with defect-dominated growth.

An increase in the fitting exponent (β or α) with temperature was also found for para-sexiphenyl islands on SiO₂, though likely for reasons [34] unrelated to the above or to increasing surface diffusion allowing for larger islands, as for a homogeneous substrate. (Further work [35] on this system found that the value of i obtained from the

---

[5] Explicitly, these coefficients are: $a_\beta = 2\Gamma\left(\frac{\beta+2}{2}\right)^{\beta+1} \Big/ \Gamma\left(\frac{\beta+1}{2}\right)^{\beta+2}$ and $b_\beta = \left[\Gamma\left(\frac{\beta+2}{2}\right) \Big/ \Gamma\left(\frac{\beta+1}{2}\right)\right]^2$.

[6] Miyamoto et al. [30] comment that capture zone analysis becomes relevant only once the density of islands is such that the area of a circle having the diffusion length as its radius becomes comparable to the mean area of the capture zones.
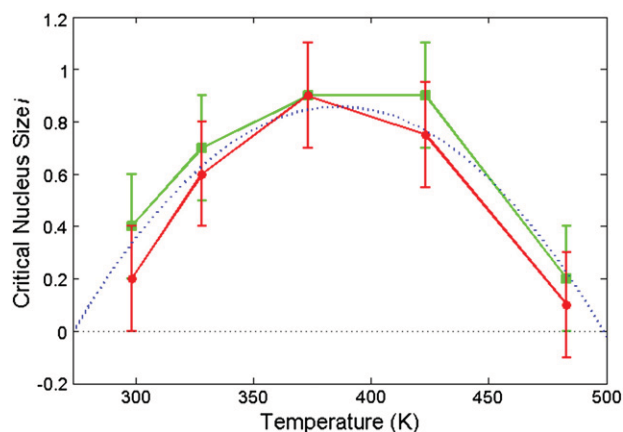
Fig. 4. Temperature dependence of critical nucleus size i extracted from the fitted values of β using the gamma distribution (green/gray squares) and the GWD (red/black circles). A parabola fit by least squares to these data has a peak between 384–388 K with 95% confidence. (For interpretation of the references to color in this figure legend, the reader is referred to the web version of this article.)

CZD using $P_\beta(s)$ is consistent with that obtained by analyzing the ISD with an empirical formula proposed by Amar and Family [18]). The decreasing portion of the curve is more difficult to describe. Pimpinelli and Ferrando [32] reported reminiscent reentrant behavior for epitaxial island growth as a function of what amounts to increasing temperature; however, their observations seem more appropriate to larger values of i than in our case, so that edge diffusion effects play a role. Note also that codeposited impurities can increase or decrease the critical nucleus size, depending on the physical role they play [29,36].

5. Summary

We have measured the growth regime of C_{60} on UTO in which monomers or dimers are the preferred island. The dependence of critical island size on temperature seems due to surface defects. The observed island behavior can be applied to organic device preparation techniques and underscores the usefulness of capture zone distribution analysis to characterize thin film nucleation and growth.

Acknowledgments

References

[1] W. Brütting, M. Bronner, M. Götzenbrugger, A. Opitz, Macromol. Symp. 268 (2008) 38.
[2] D.S. Germack, C.K. Chan, B.H. Hamadani, L.J. Richter, D.A. Fischer, D.J. Gundlach, D.M. DeLongchamp, Appl. Phys. Lett. 94 (2009) 233303.
[3] S.S. Lee, Y.-L. Loo, Annu. Rev. Chem. Bio. Eng. 1 (2010) 59.
[4] O.D. Jurchescu, D.A. Mourey, S. Subramanian, S.R. Parkin, B.M. Vogel, J.E. Anthony, T.N. Jackson, D.J. Gundlach, Phys. Rev. B 80 (2009) 085201.
[5] T. Arai, Y. Murakami, H. Suematsu, K. Kikuchi, Y. Achiba, I. Ikemoto, Solid State Comm. 84 (1992) 827.
[6] E. Frankevich, Y. Maruyama, H. Ogata, Chem. Phys. Lett. 214 (1993) 39.
[7] B.R. Conrad, W.G. Cullen, W. Yan, E.D. Williams, Appl. Phys. Lett. 91 (2007) 242110.
[8] I. Salzmann, S. Duhm, R. Opitz, R.L. Johnson, J.P. Rabe, N. Koch, J. Appl. Phys. 104 (2008) 114518.
[9] S. Kobayashi, T. Takenobu, S. Mori, A. Fujiwara, Y. Iwasa, Appl. Phys. Lett. 82 (2003) 4581.
[10] R.C. Haddon, A.S. Perel, R.C. Morris, T.T.M. Palstra, A.F. Hebard, R.M. Fleming, Appl. Phys. Lett. 67 (1995) 121.
[11] B.R. Conrad, W.G. Cullen, B.C. Riddick, E.D. Williams, Surf. Sci. 603 (2009) L27.
[12] H. Watanabe, T. Baba, M. Ichikawa, Jpn. J. Appl. Phys. 39 (2000) 2015.
[13] R. Hasunuma, A. Ando, K. Miki, Y. Nishioka, Appl. Surf. Sci. 162–163 (2000) 547.
[14] H.W. Kroto, A.W. Allaf, S.P. Balm, Chem. Rev. 91 (1991) 1213.
[15] J. Tersoff, D.R. Hamann, Phys. Rev. Lett. 50 (1983) 1998.
[16] J.A. Venables, G.D.T. Spiller, M. Hanbücken, Rep. Prog. Phys. 47 (1984) 399.
[17] J.W. Evans, P.A. Thiel, M.C. Bartelt, Surf. Sci. Rep. 61 (2006) 1.
[18] J.G. Amar, F. Family, Phys. Rev. Lett. 74 (1995) 2066.
[19] P.A. Mulheran, J.A. Blackman, Phys. Rev. B 53 (1996) 10261.
[20] D. Weaire, J.P. Kermode, J. Wejchert, Philos. Mag. B 53 (1986) L101.
[21] N.L. Johnson, S. Kotz, N. Balakrishnan, Gamma distributions, second ed., Continuous Univariate Distributions, vol. 1, Wiley, New York, 1994, p. 337.
[22] T. Kiang, Z. Astrophys. 64 (1966) 433.
[23] A. Pimpinelli, T.L. Einstein, Phys. Rev. Lett. 99 (2007) 226102.
[24] A.Y. Abul-Magd, Physica A 368 (2006) 536.
[25] A. Pimpinelli, T.L. Einstein, Phys. Rev. Lett. 104 (2010) 149602.
[26] M. Li, Y. Han, J.W. Evans, Phys. Rev. Lett. 104 (2010) 149601.
[27] F. Shi, Y. Shim, J.G. Amar, Phys. Rev. E 79 (2009) 011602.
[28] D.L. González, A. Pimpinelli, T.L. Einstein, Phys. Rev. E 84 (2011) 011601.
[29] R. Sathiyanarayanan, B.H. Hamouda, A. Pimpinelli, T.L. Einstein, Phys. Rev. B 83 (2011) 035424.
[30] S. Miyamoto, O. Moutanabbir, E.E. Haller, K.M. Itoh, Phys. Rev. B 79 (2009) 165415.
[31] C. Ratsch, A. Zangwill, P. Šmilauer, D.D. Vvedensky, Phys. Rev. Lett. 72 (1994) 3194.
[32] A. Pimpinelli, R. Ferrando, Phys. Rev. B 60 (1999) 17016.
[33] B.R. Conrad, Gomar-Nadal Elba, W.G. Cullen, A. Pimpinelli, T.L. Einstein, E.D. Williams, Phys. Rev. B 77 (2008) 205328.
[34] S. Lorbek, G. Hlawacek, C. Teichert, Eur. Phys. J. Appl. Phys. 55 (2011) 23902.
[35] T. Potocar, S. Lorbek, D. Nabok, Q. Shen, L. Tumbek, G. Hlawacek, P. Puschnig, C. Ambrosch-Draxl, C. Teichert, A. Winkler, Phys. Rev. B 83 (2011) 075423.
[36] M. Kotrla, J. Krug, P. Šmilauer, Phys. Rev. B 62 (2000) 2889.